Biological Cybernetics (2019) 113:239–255
https://doi.org/10.1007/s00422-018-00790-6

Biological Cybernetics

ORIGINAL ARTICLE

Representation of object's shape by multiple electric images in electrolocation

Kazuhisa Fujita[1,2] · **Yoshiki Kashimori**[2]

Received: 11 March 2018 / Accepted: 21 December 2018 / Published online: 10 January 2019

Abstract
Weakly electric fish generate an electric field by discharging an electric organ located on the tail region. An object near the fish modulates the self-generated electric field. The modulated field enables the fish to perceive objects even in complete darkness. The ability to perceive objects is provided by the electrosensory system of the fish. Electroreceptors distributed on the fish's skin surface can sense the modulated field, on the basis of transdermal voltage across the skin surface, called electric images. The fish can extract object's features such as lateral distance, size, shape, and electric property from an electric image. Although previous studies have demonstrated the relationship between electric-image features and object's distance and size, it remains unclear what features of an electric image represent the object's shape. We make here a hypothesis that shape information is not represented by a single image but by multiple images caused by the object's rotation or fish movement around the object. To test the hypothesis, we develop a computational model that can predict electric images produced by the rotation of differently shaped objects. We used five different shapes of resistive objects: a circle, a square, an equilateral triangle, a rectangle, and an ellipsoid. We show that differently shaped objects of a fixed arrangement generate similar Gaussian electric images, irrespective of their shapes. We also show that the features of an electric image such as the peak amplitude, half-maximum width, and peak position exhibit the angle-dependent variations characteristic to object rotation, depending on object shapes and lateral distances. Furthermore, we demonstrate that an integration effect of the peak amplitude and half-maximum width could be an invariant measure of object shape. These results suggest that the fish could perceive an object shape by combining those image features produced during exploratory behaviors around the object.

Keywords Electrolocation · Finite-element model · Electric image · Object's shape · Object rotation

1 Introduction

Weakly electric fish generate an electric field by discharging an electric organ (EO) located on the tail region. Wave-type electric fish have a quasisinusoidal, wave-type electric organ discharge (EOD), and pulse-type fish have a pulse-type EOD separated by intervals. Objects with electric properties different from those of surrounding water modulate the electric field around the fish body (Lissmann and Machin 1958). The electroreceptors distributed on the fish's skin surface monitor the state of the electric field modulation, on the basis of the spatio and temporal patterns of transdermal potential perturbation called by electric images. The electroreceptor system allows the fish to detect, identify, and localize an object in its environment even in complete darkness (Bastian 1981; Heiligenberg 1991; von der Emde et al. 1998). To understand the mechanism of electrolocation, we need to know the profiles of an unperturbed electric field around the fish body and of fields perturbed by objects.

Electric images generated by an object depend on the object's features such as distance, size, shape, and electric properties. The fish can detect such object's features from the electric image. Experimental studies have demonstrated how electric images are modulated by these object's features. The electric organ discharges and the electric fields perturbed by spherical objects were measured by previous studies (Bastian

Communicated by André Longtin.

✉ Kazuhisa Fujita
kazu@spikingneuron.net

[1] Department of Clinical Engineering, Faculty of Health Sciences, Komatsu University, 10 - 10 Doihara-Machi, Komatsu, Ishikawa 923-0921, Japan

[2] Department of Engineering Science, University of Electro-Communications, 1-5-1 Chofugaoka, Chofu, Tokyo 182-8585, Japan

1981; Rasnow 1996; Rasnow and Bower 1996; Assad et al. 1998). Assad et al. (1999) showed that the lateral distance of a spherical object can be determined by the relative width of electric image, irrespective of the sphere's size. Object size can be determined unambiguously from the relative width, the sphere's impedance, and the peak amplitude of an electric image (Rasnow 1996; Assad et al. 1999). Moreover, in the pulse-type fish, *G. Petersii*, the maximum slope normalized by the maximum amplitude has been shown to be a useful measure to represent objects distance (von der Emde et al. 1998). In terms of the discrimination of object's capacitance, von der Emde (1998) demonstrated the dependences of the peak amplitude and phase shift of an electric image on object's capacitance. Furthermore, recent studies have shown that the pulse-type fish, *G. Petersii*, can discriminate between differently shaped objects (von der Emde and Fetz 2007; von der Emde et al. 2010). However, it remains unclear what features of an electric image represent object's shape.

Modeling study plays a complementary role in understanding the relationship between object's features and electric-image features because it is difficult to accurately measure the electric field around a fish body and electric images in an experimental setting. Some modeling and theoretical studies have shown the electric fields induced by resistive objects (Heiligenberg 1975; Hoshimiya et al. 1980; Bacher 1983; Rasnow 1996; Caputi et al. 1998; Assad et al. 1999; Rother et al. 2003; Migliaro et al. 2005; Chen et al. 2005; Babineau et al. 2006, 2007). These studies revealed the geometry of an unperturbed field and the dependences of the peak amplitude and width of an electric image on object's distance and its size. We also offered a computational model that can predict the phase and amplitude modulations of electric images generated by objects with complex impedance (Fujita and Kashimori 2010). To our knowledge, our model was the first to show the phase modulation of electric images besides the amplitude modulation in a wave-type fish. Furthermore, a mathematical model was proposed for active electrolocation of the fish (Ammari et al. 2013), and studies on robotics inspired by electric sense demonstrated that active sensing of sensor robots enables these robots to accurately estimate the location and size of objects (Solberg et al. 2008; Alamir et al. 2010; Boyer et al. 2012, 2013; Boulier 2013; Bai et al. 2015; Lanneau et al. 2016; Bazeille et al. 2017; Lanneau 2017) and their capacitive properties (Bai et al. 2016). In addition, sensor robots can also electrolocate an object using electro-navigations and exploratory behaviors, controlled by a Kalman filter (Lebastard et al. 2012, 2013) and other algorithms (Lebastard et al. 2016; Bazeille et al. 2018). For motion-controlled systems equipped with electric sense, see the short review (Boyer and Lebastard 2018). However, there are few modeling studies that aim to elucidate how weakly electric fish perceive object's shapes in the natural environment.

In this study, we examine what features of an electric image represent object's shape. We assume that weakly electric fish may perceive an object's shape using multiple electric images caused by rotation movement of the fish around the object. We investigate the multiple images generated by an object rotation, instead of rotation movement of the fish around the object. The multiple images are produced for various angles made by the orientations of an object and the electric organ. We developed a computational model for electric fields generated by the rotation of differently shaped objects. Square objects and an equilateral-triangle one were used to investigate the effect of corner angle on the electric image produced by these objects. Also, two elongated objects, a rectangle object and an ellipsoidal one, were used to investigate how elongated shapes affect the electric images. We show that electric images elicited by objects have similar Gaussian shapes, independently of their shapes. We also show that the maximum amplitude, relative width, and peak position of the electric image exhibit the angle dependences characteristic to the rotations of differently shaped objects. Furthermore, we demonstrate that an integration effect of the peak amplitude and half-maximum width could be an invariant measure for shape discrimination.

2 A computational model for calculating an electric field

2.1 A model of fish body and a nearby object in a water tank

Figure 1 shows a model of the fish body and a nearby object in a water tank. The electric fish and the nearby object were put in the two-dimensional rectangular water tank. The size of the water tank was 700 mm × 500 mm. The fish body was approximated as a rectangle object (200 mm × 8 mm). The model of fish consists of the interior tissue of the fish body, the skin with a high resistivity, and the electric organ constructed with an electric dipole. Each of the three domains has a uniform resistivity. The resistivity of the interior tissue and the skin is 0.1 and 120 kΩ · cm, respectively. The resistivity of water is 3.8 kΩ · cm. These values are the same as those used in the previous studies (Hoshimiya et al. 1980; Fujita and Kashimori 2010). Although the skin also has a capacitive component (Hoshimiya et al. 1980), we ignored the capacitive current across the skin because the resistive current across the skin is sufficiently large compared with the capacitive current. Similarly, the capacitive components of other domains were neglected because the capacitive current makes little contribution to the total current. The dipole, shown by the open circles in Fig. 1, has the radius of 1 mm and is represented by the two poles located at (370 mm, 254 mm) and (430 mm, 254 mm), where the origin of the coor-

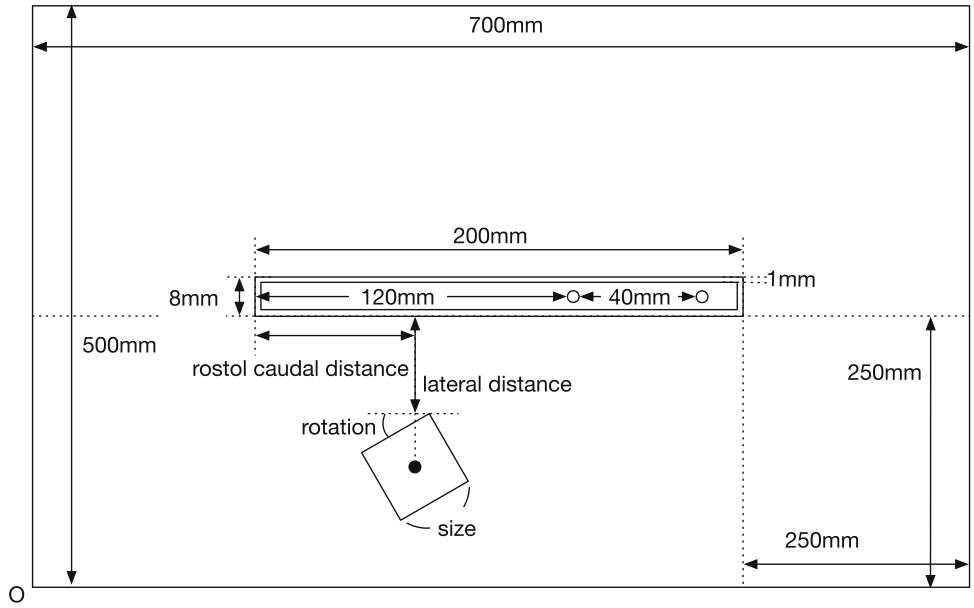

Fig. 1 Model of a weakly electric fish and a nearby object in a water tank. The fish was put on the center of the water tank whose size is 700×500 mm. The fish body is approximated with a rectangular shape with the size of 200×8 mm, and an electric organ located in the caudal region is modeled with a dipole depicted by the small open circles. An object is placed on a rostro-caudal location and at a lateral distance. The object is rotated in the counter-clockwise direction, and the rotation angle is measured with reference to the arrangement that a sideline of the object, facing the fish boy, is in parallel with the longitudinal axis of the fish body

dinates is defined by the position of the lower left corner of the tank. The electric potentials of the two poles were set at ± 12.5 mV (Hoshimiya et al. 1980; Fujita and Kashimori 2010) and was kept constant. The dipole generates the electric field around the fish body. Moreover, the boundary condition was determined so that the electric potential converges to an asymptotic value of 0mV at the four boundaries of the water tank.

Also, we used only resistive objects that have five object's shapes, or square, triangle, circle, rectangle, and ellipse. The resistivity of the objects is $1.0 \times 10^{-4}\ \Omega \cdot$cm. Although plastic objects are commonly used in the experiments of electrolocation, they generate electric images similar to those generated by metal objects, except for the opposite changes in electric-image amplitude to those of metal objects (Chen et al. 2005). Thus we consider only the electric images generated by metal objects.

2.2 A mathematical model of an electric field around a fish body

We present here a computational model for calculating the electric field generated by the weakly electric fish and the fields modulated by an object. In a natural environment, it is difficult to accurately measure the electric field generated by the fish and those modulated by an object. Thus modeling study provides a complementary method for understanding the geometrical property of the electric field around the fish and the relationship between the modulation of electric field and object's features. Previous studies have developed computational models for calculating the electric field and investigated the properties of the unperturbed field and of the fields modulated by an object (Heiligenberg 1975; Hoshimiya et al. 1980; Bacher 1983; Rasnow 1996; Caputi et al. 1998; Assad et al. 1999; Rother et al. 2003; Migliaro et al. 2005; Chen et al. 2005; Babineau et al. 2006, 2007). There are also a theoretical study (Ammari et al. 2013) and studies on robotics inspired by the electric sense (Solberg et al. 2008; Alamir et al. 2010; Boyer et al. 2012, 2013; Boulier 2013; Bai et al. 2015, 2016; Lanneau et al. 2016; Bazeille et al. 2017; Lanneau 2017). Of these models, the finite-element method (FEM) has been used to calculate the electric field perturbed by the fish and an object because this method is easily tractable for electric field calculation (Heiligenberg 1975; Hoshimiya et al. 1980; Chen et al. 2005; Babineau et al. 2006, 2007; Fujita and Kashimori 2010).

The electric field of the water tank including an electric fish, $\boldsymbol{E}$, is determined by Ohm's law:

$$\boldsymbol{E} = \rho \boldsymbol{j}, \tag{1}$$

where $\boldsymbol{E}$ is electric field, $\boldsymbol{j}$ is current density, and ρ is resistivity. Because of $E = -\nabla V$, the potential V is given by

$$\nabla V = -\rho \boldsymbol{j}. \tag{2}$$

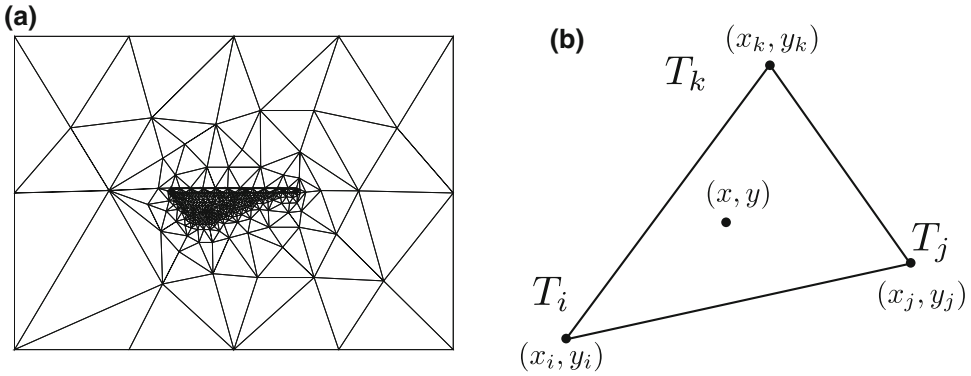

Fig. 2 **a** Mesh space formed for the computation of electric field. The mesh space consists of triangle elements of various sizes. The square object has each side of 30 mm and has only a resistivity. **b** A triangle element and a given point within the triangle element. Electric potential at the point (x, y) is calculated by a linear interpolation of the electric potentials at the three points, (x_i, y_i), (x_j, y_j),and (x_k, y_k)

We solve Eq. 2 to obtain the electric potentials at all locations in the water tank.

We used the FEM to calculate the electric field generated by the fish and the field perturbed by a nearby object. Because Eq. 2 is similar to the heat spread equation, we are easily able to apply the FEM to the electric field calculation. The calculation of the electric field by the FEM consists of three calculation stages; preprocessing, processing, and postprocessing.

2.3 Preprocessing

In preprocessing, we make a mesh space to solve Eq. 2 determining the electric potential in the water tank including the fish and an object. The space of water tank is discretized by many elements and is converted to a mesh network. We used an open free soft, Free FEM++, to make the mesh network in the water tank. Figure 2a shows a mesh space in the water tank including the fish and a nearby square object. The mesh space nearby the fish and the object has the dense distribution of smaller sizes of the element, while that far away from the fish and the object is constructed with the sparse distribution of large sizes of elements. The mesh space is shaped for each rotation of an object. The mesh space by the FEM++ is made by a self-organized process based on the geometry of an object and gives accuracy enough for the calculation of an electric image of a rotated object because the mesh space is formed based on the lines of different angles composing the rotated object. On the other hand, the mesh spaces composed of well-used mesh units such as homogeneous square and triangle units do not have enough accuracy for object rotation.

2.4 Processing

In processing, we calculate the potentials of all nodes of the mesh. The nodal potential is defined by the vector, $\{\boldsymbol{V}\} = \{V_1, V_2, \ldots, V_i, \ldots, V_N\}^{\mathrm{T}}$, where V_i is the potential of the ith node. The nodal potential, $\boldsymbol{V}$, is determined by the following equation:

$$[\boldsymbol{K}]\{\boldsymbol{V}\} = \{\boldsymbol{0}\}, \tag{3}$$

where $[\boldsymbol{K}]$ is the $N \times N$ conductivity matrix. The vector, $\{\boldsymbol{0}\}$, means that the total electric current flowing to each node is zero. The elemental $[\boldsymbol{K}]_e$ matrix for the eth triangle element can be written as

$$\begin{aligned}[\boldsymbol{K}]_e &= \begin{bmatrix} K^e_{ii} & K^e_{ji} & K^e_{ki} \\ K^e_{ij} & K^e_{jj} & K^e_{kj} \\ K^e_{ik} & K^e_{jk} & K^e_{kk} \end{bmatrix} \\ &= \frac{t}{4A}\left\{ k_x \begin{bmatrix} b_i^2 & b_i b_j & b_i b_k \\ b_i b_j & b_j^2 & b_j b_k \\ b_i b_k & b_j b_k & b_k^2 \end{bmatrix} \right. \\ &\quad \left. + k_y \begin{bmatrix} c_i^2 & c_i c_j & c_i c_k \\ c_i c_j & c_j^2 & c_j c_k \\ c_i c_k & c_j c_k & c_k^2 \end{bmatrix} \right\}, \end{aligned} \tag{4}$$

where the ith, the jth, and the kth nodes compose a triangle element, k_x and k_y are electrical conductivity $[\Omega^{-1}\mathrm{mm}^{-1}]$ of the triangle element, t is the thickness of the element, and b_L and $c_L (L = i, j, k)$ are constants for a given triangle element. In this study, we set $t = 1$ mm. We obtain $k_x = k_y = 1/R$, where R is resistivity. A is defined as

$$\begin{aligned} 2A &= \det \begin{bmatrix} 1 & x_i & y_i \\ 1 & x_j & y_j \\ 1 & x_k & y_k \end{bmatrix} \\ &= (x_i y_j - x_j y_i) + (x_j y_k - x_k y_j) + (x_k y_i - x_i y_k), \end{aligned} \tag{5}$$

where b_L and $c_L (L = i, j, k)$ are denoted by

$$\begin{aligned} b_i &= y_j - y_k; \quad c_i = x_k - x_j; \\ b_j &= y_k - y_i; \quad c_j = x_i - x_k; \\ b_k &= y_i - y_j; \quad c_k = x_j - x_i; \end{aligned} \quad . \tag{6}$$

We explain the relation between K and K_e using the following example. In the example, the mesh consist of two triangles. The triangle elements 1 and 2, respectively, have the nodes $i = 1$, $j = 2$, $k = 3$ and $i = 2$, $j = 3$, $k = 4$. The elemental $[\boldsymbol{K}]_1$ and $[\boldsymbol{K}]_2$ are denoted by

$$[\boldsymbol{K}]_1 = \begin{bmatrix} K^1_{11} & K^1_{21} & K^1_{31} \\ K^1_{12} & K^1_{22} & K^1_{32} \\ K^1_{13} & K^1_{23} & K^1_{33} \end{bmatrix}$$

and

$$[\boldsymbol{K}]_2 = \begin{bmatrix} K^2_{22} & K^2_{32} & K^2_{42} \\ K^2_{23} & K^2_{33} & K^2_{43} \\ K^2_{24} & K^2_{34} & K^2_{44} \end{bmatrix}.$$

We obtain the conductivity matrix $[K]$,

$$[\boldsymbol{K}] = \begin{bmatrix} K^1_{11} & K^1_{21} & K^1_{31} & 0 \\ K^1_{12} & K^1_{22} + K^2_{22} & K^1_{32} + K^2_{32} & K^2_{42} \\ K^1_{13} & K^1_{23} + K^2_{23} & K^1_{33} + K^2_{33} & K^2_{43} \\ 0 & K^2_{24} & K^2_{34} & K^2_{44} \end{bmatrix}.$$

Thus, the element of the conductivity matrix K_{nm} is summation of K^e_{nm}.

We obtain the nodal potential by solving this multi-dimensional simultaneous linear equations (Eq. 3). Details of the derivation of these formula are shown in Lewis et al. (2004).

2.5 Postprocessing

In postprocessing, we calculate the electric potentials of all locations in the water tank using a linear interpolation based on the results calculated by the processing. The potential at the position (x, y) within the triangle element constructed with the three nodes i, j, and k, shown in Fig. 2b, is denoted by

$$V(x, y) = \alpha_1 + \alpha_2 x + \alpha_3 y. \tag{7}$$

The polynomial is linear in x and y, and contains three coefficients, α_1, α_2, and α_3. Since the triangle shown in Fig. 2b has the three lines connecting the three nodes, the coefficients, α_1, α_2, and α_3, are determined by

$$\alpha_1 = \frac{1}{2A}[(x_j y_k - x_k y_j)V_i + (x_k y_i - x_i y_k)V_j + (x_i y_j - x_j y_i)V_k], \tag{8}$$

$$\alpha_2 = \frac{1}{2A}[(y_j - y_k)V_i + (y_k - y_i)V_j + (y_i - y_j)V_k], \tag{9}$$

$$\alpha_3 = \frac{1}{2A}[(x_k - x_j)V_i + (x_i - x_k)V_j + (x_j - x_i)V_k]. \tag{10}$$

With these equations, we can obtain the electric potentials at all positions in the water tank. The spatial resolution was set at 0.5 mm.

2.6 Electric image

Electroreceptors monitor the state of electric potential modulations, on the basis of spatio and temporal changes of transdermal potential across the fish skin, called electric images. The fish can detect an object from the difference between transdermal potentials in the presence and in the absence of an object. The transdermal potential along the rostro-caudal axis x, $V_{\mathrm{tr}}(x)$, is the difference between external and internal potential, denoted by

$$V_{\mathrm{tr}}(x) = V_{\mathrm{ext}}(x) - V_{\mathrm{int}}(x), \tag{11}$$

where "ext" and "int" indicate the exterior and interior boundaries of the fish's skin, respectively. Then the electric image, $V_{\mathrm{img}}(x)$, can be calculated by

$$V_{\mathrm{img}}(x) = V^{\mathrm{obj}}_{\mathrm{tr}}(x) - V^{\mathrm{noobj}}_{\mathrm{tr}}(x), \tag{12}$$

where $V^{\mathrm{obj}}_{\mathrm{tr}}(x)$ and $V^{\mathrm{noobj}}_{\mathrm{tr}}(x)$ are the transdermal potentials in the presence and in the absence of an object, respectively.

3 Results

3.1 Geometry of electric fields modulated by fish body and an object

Figure 3a shows the electric field around a fish body in the absence of an object, or the basal (unperturbed) potential field. The field has a positive and a negative area that are divided by zero-isopotential lines. The sign of the field potential is alternatively changed with a sinusoidal oscillation of dipole charges. The potential field around the fish body was modulated by an electric property of the fish body. The calculated field potential reproduces several qualitative aspects shown in the previous modeling studies (Heiligenberg 1975; Hoshimiya et al. 1980; Assad et al. 1999; Chen et al. 2005; Babineau et al. 2006) and the experimental studies (Bastian 1981; Rasnow and Bower 1996; Assad et al. 1998; Chen et al. 2005); rostrally extended potential and homogeneous potential in the rostral side. Figure 3b, c shows the electric field evoked by a square object with the rotation angle of 0° and that generated by the square object rotated by 30°, respectively. These objects, respectively, evoked local modulations of electric fields characteristic to the object's orientation. Figure 3d, e shows the differences between the electric fields generated by these objects and the basal potential. These objects produced local modulations of the electric field in

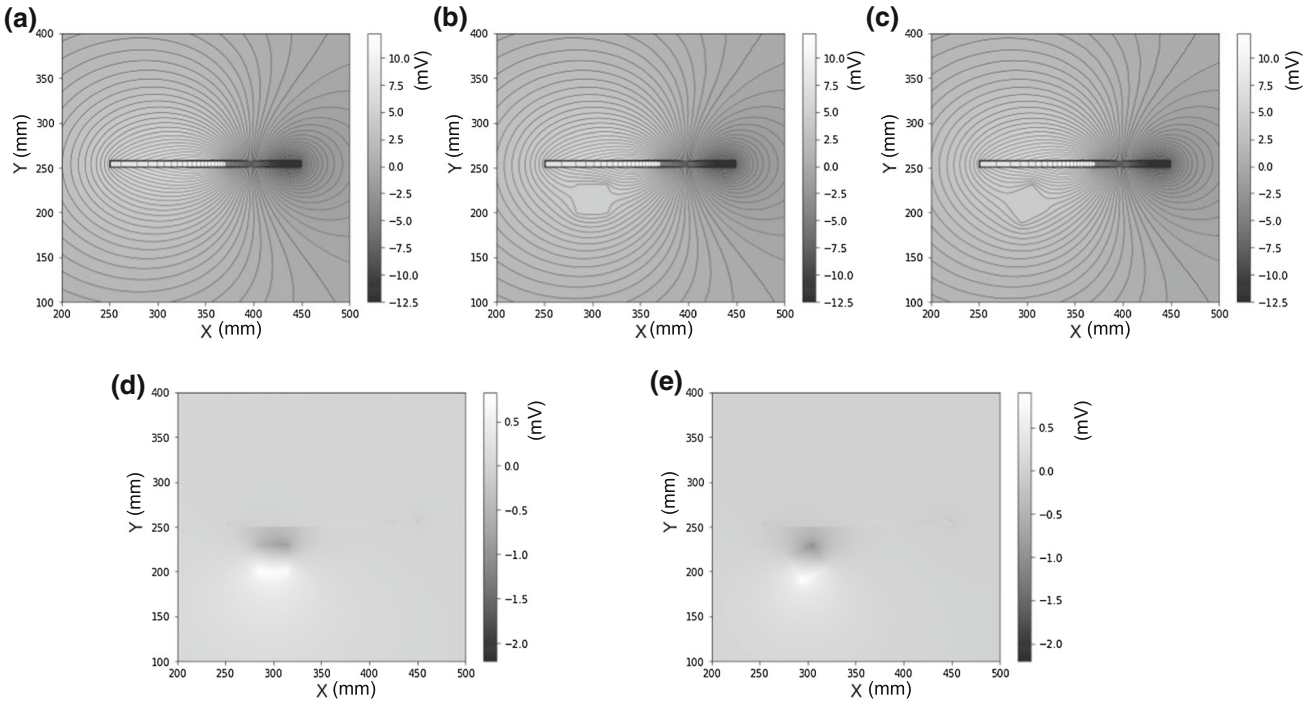

Fig. 3 **a**–**c** Electric fields around a fish body. **a** Unperturbed field. **b**, **c** Electric fields perturbed by a square with the rotation angle of 0° (**b**) and that rotated by 30° (**c**). The square object has each side of 30 mm. **d**, **e** Potential differences between the unperturbed field and the fields modulated by the unrotated square object (**d**) and that rotated by 30° (**e**)

front and back side of each object, depending on the object's orientation.

3.2 Characteristics of electric images elicited by differently shaped objects

Figure 4a shows the electric images elicited by three objects of different shapes, placed at five different distances lateral to the fish body surface. The lateral distance is defined by the minimum distance between an object and the fish body surface, as shown in Fig. 1. The objects used were a square object of 30 mm each side, an equilateral-triangle object of 30 mm each side, and a circle object of the diameter of 30 mm. The center of mass of each object was placed at the rostro-caudal position of 50 mm. The electric images evoked exhibited slightly distorted Gaussian shapes independently of the object's shapes. The corners of the square and triangle objects have different sharpness, but yielded the similar "blurred" images irrespective of object's shapes, in contrast to inputs in visual systems. This indicates that the difference in object's shapes is not explicitly reflected by the difference in the shape of a single electric image. The peak amplitude of the electric images was significantly reduced for the lateral distances of 10–40 mm, while it was gradually decreased for the lateral distances larger than 40 mm. The peak amplitudes for the lateral distances of 40 and 50 mm were extremely small compared with that for the distance of 10 mm. On the other hand, the peak position of electric images was differently shifted depending on these object's shapes: the circle object, placed at different lateral distances, almost unchanged the peak position corresponding to the center position of the object, whereas the square and triangle objects produced the peak shifts toward the caudal side of fish body, reducing with the increase in lateral distances. These shifts may be caused by some feature of object's shape. The square and triangle objects have a corner orienting toward the electric organ located in the caudal region, which makes a dominant contribution of electric image formation. As a result, the presence of the corner yields the caudal shifts of the peak position. In contrast, the circle lacking such a corner does not evoke the caudal shift. Figure 4b shows the electric images distributed on the fish body surface in the case where the three objects were placed at various rostro-caudal locations. The rostro-caudal location was measured from the edge of fish's head, as shown in Fig. 1. An object was put at the rostro-caudal location that corresponds to the center of the object. The peak positions of electric images elicited by the circle object nearly matched the object positions except for the caudal shifts for the object positions of 10 and 20 mm. The caudal peak shifts could be due to the edge effect of the head region. In contrast, the peak positions of electric images generated by the square and triangle objects were more shifted toward the caudal side because of a corner orienting to the electric organ. Figure 4c shows the effect of object size on the electric images. The

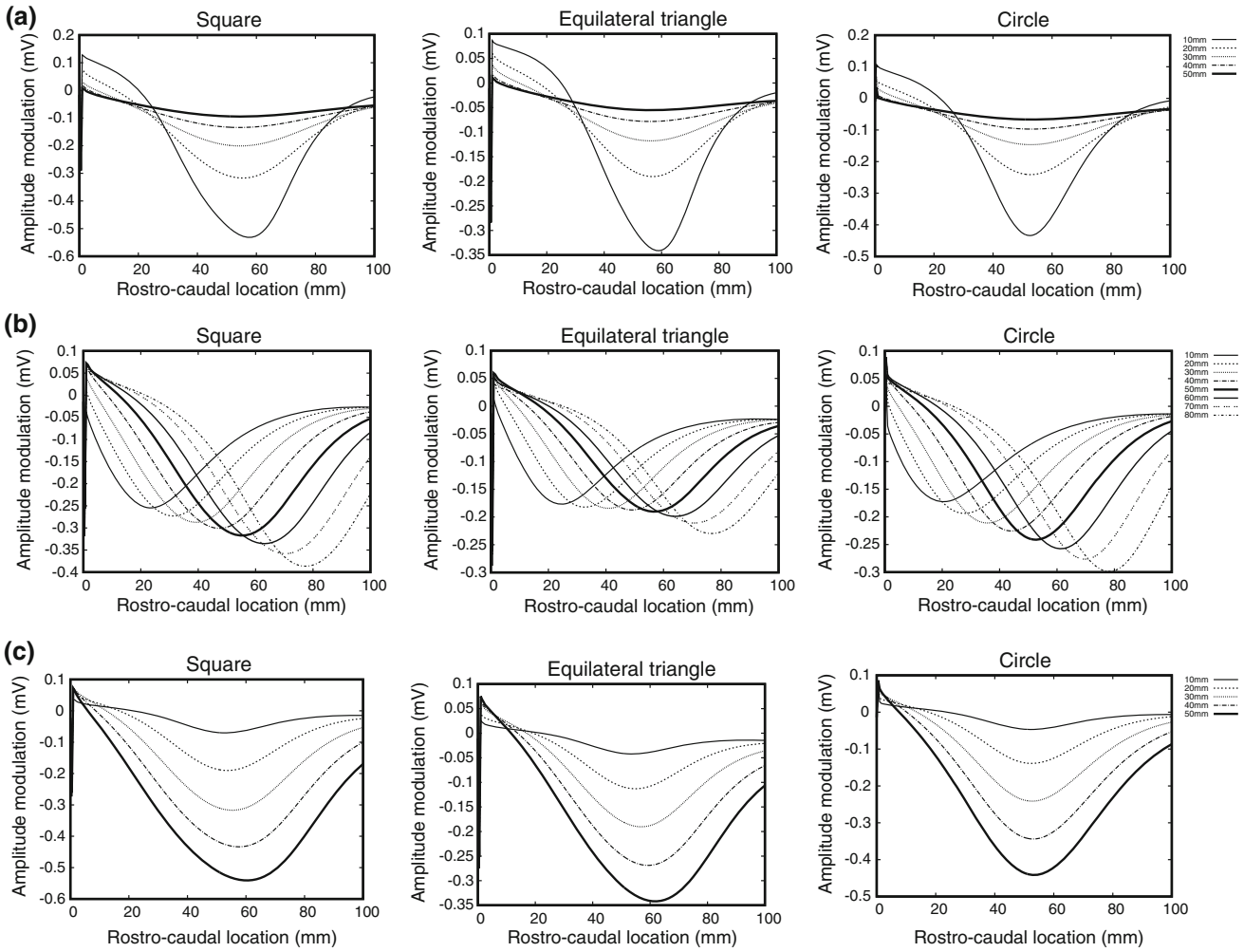

Fig. 4 Effects of lateral distance, rostro-caudal location, and size of objects on electric images. **a–c** Electric images evoked by objects of three different shapes under different conditions. These curves in **a–c** were calculated with the step of 1 mm in rostro-caudal location. In **a** and **b** three objects were used: a circle with the diameter of 30 mm, a square with each side of 30 mm, and an equilateral triangle with each side of 30 mm. In **a** the lateral distance was varied under the condition that the object center was fixed at the rostro-caudal location of 50 mm, and in (**b**) the rostro-caudal location was varied under the condition that the lateral distance was fixed at 20 mm. In **c** the object size was varied. The lateral distance and the rostro-caudal location were fixed at 20 mm and 50 mm, respectively

peak amplitude increased monotonically with increasing the object size, irrespective of object's shape. The peak locations of the electric images elicited by the circle object remained almost unchanged, while the peak locations evoked by the square and triangle object were more shifted toward the caudal side with increasing the object size. These shifts are due to the corner effect similar to the effect discussed in the peak shifts for lateral distance. The decrease in the object size led to a reduction in the peak shift because the corner effect is weakened.

Figure 5a, b shows the dependences of the peak amplitude and half-maximum width (HMW) of electric images on object size, respectively. The peak amplitude and HMW are key features determining the Gaussian modulation. Objects of three different shapes were used and were placed at the lateral distance of 20 mm. The increase in object size caused the increases in the peak amplitude and broadness in the electric images. The change of object size provided the linear dependences on these features, irrespective of object shape. Figure 5c, d, respectively, shows the effects of lateral distance on the peak amplitude and HMW of electric images, produced by three different object shapes. The peak amplitudes generated by the three objects were exponentially decreased with increasing the lateral distance, and then they appeared to converge asymptotically to the value of 0. At the lateral distances larger than 40 mm, the peaks elicited by the three objects were significantly smaller than that at the lateral distance of 10 mm, and came closer to each other, implicating that it would be difficult to discriminate between the circle, square, and triangle shapes. Also, the HMW elicited by the

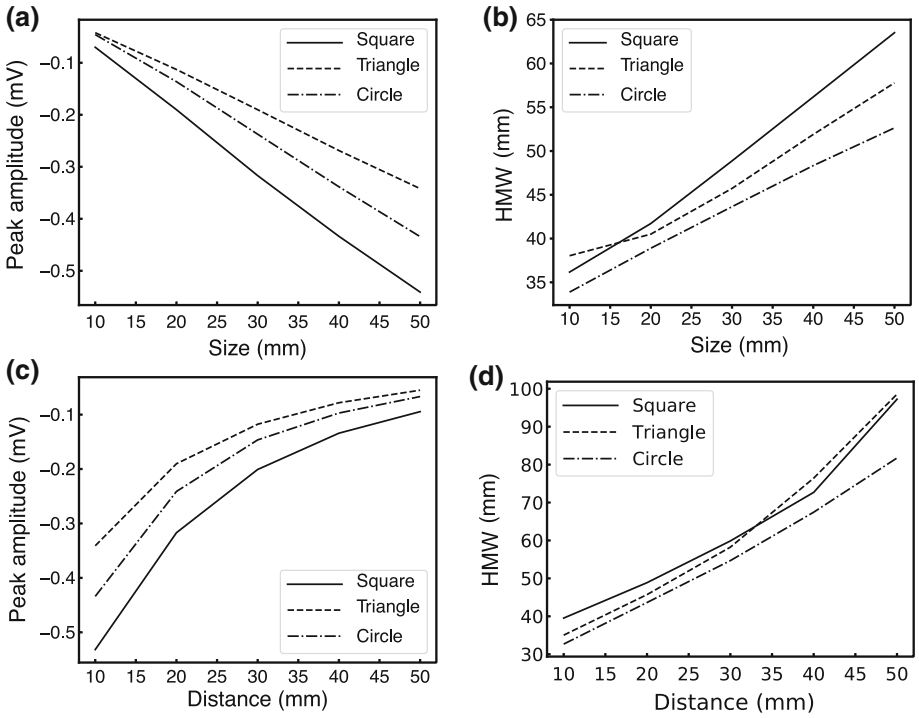

Fig. 5 Effects of object size and lateral distance on the peak amplitude and half-maximum width (HMW) of the electric image. **a**, **b** Object size. **c**, **d** Lateral distance. Three different shapes, circle, square, and triangle, were used. In **a**, **b** object size was varied under the condition that the lateral distance is 20 mm and the rostro-caudal location is 50 mm. In **c**, **d** the lateral distance was varied under the condition the rostro-caudal location is 50 mm. The diameter of the circle and the side length of the square and the triangle are 30 mm

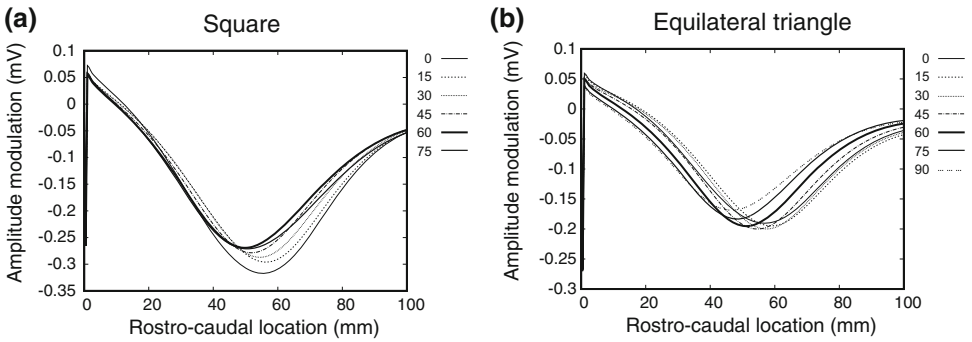

Fig. 6 Electric images generated by the rotation of two objects. **a** A square object with each side of 30 mm and **b** an equilateral-triangle object with each side of 30 mm. The objects were put at the lateral distance of 20 mm and rotated around the object center located on the rostro-caudal position of 50 mm. The numbers in the upper right in each panel represent the rotation angles

circle object was linearly increased with increasing the lateral distance, while the HMWs evoked by the square and triangle objects exhibited bilinear dependences of HMWs on object size. The increase in the lateral distance caused a significant broadness of the electric images. At the lateral distances larger than 40 mm, the electric images have the HMWs larger than 70 mm, spreading over the almost entire rostral area. Thus the electric images at the distances larger than 40 mm have smaller peaks and broader widths, making it hard for the fish to discriminate between object's shapes. The results are consistent with the behavioral study showing that a weakly electric fish is hard to discriminate between a small and a large cube and between a cube and a pyramid for the lateral distances larger than 40 mm (von der Emde et al. 2010).

3.3 Dependence of electric-image features on rotation angles of an object

Weakly electric fish change their location and orientation in exploratory behaviors. The behaviors enable the fish to generate multiple electric images necessary for discrimination of an object's shape. We consider here the effect of object rotation on electric images because object rotation is relative to the rotation movement of the fish. Figure 6a, b shows the electric images evoked by rotations of a square and an equilateral-triangle objects, respectively. These objects have the side length of 30 mm, and the location of their center of mass is the rostro-caudal location of 50 mm. Each object was rotated around the center of mass under the condition that the minimum distance between the object and the fish

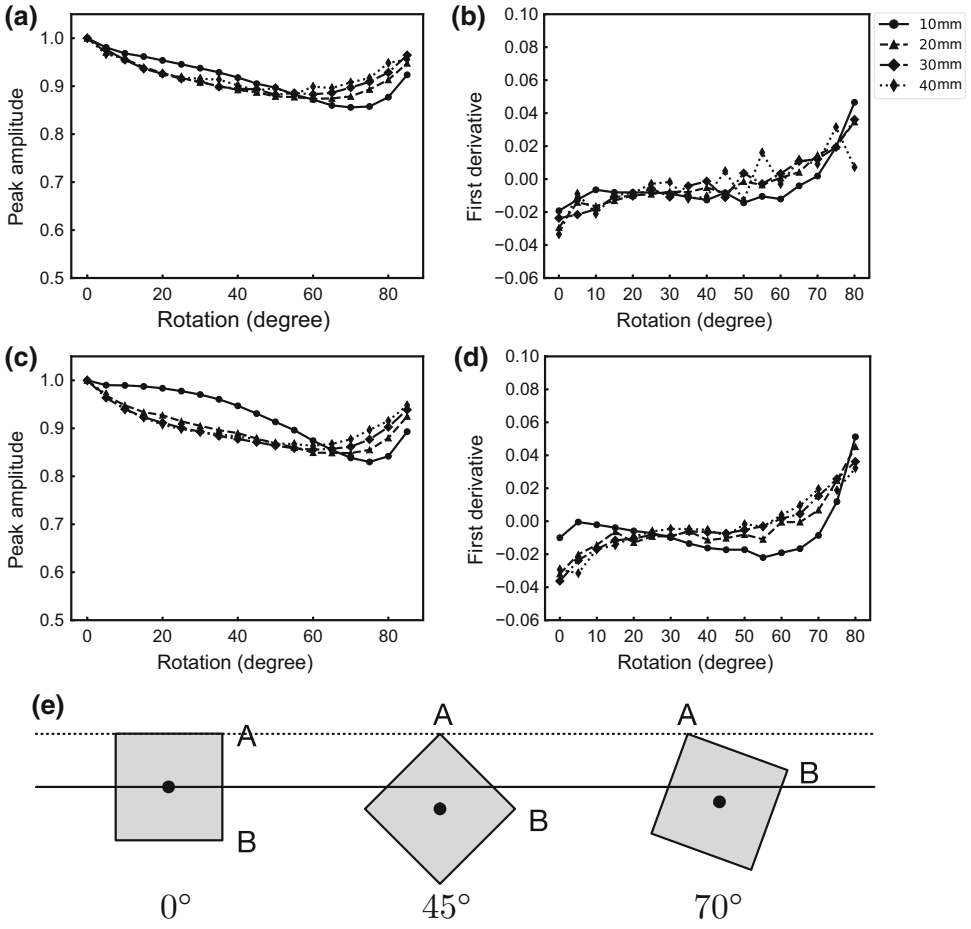

Fig. 7 Angle dependences for normalized peak amplitude of electric image and their first derivatives in the rotations of two square objects. Dependences are shown for four lateral distances of 10, 20, 30, and 40 mm. **a**, **b** Square with each side of 20 mm, and **c**, **d** that with each side of 30 mm. **e** Orientations of the square object generated by three rotation angles

body surface was kept constant. The rotation of the square object by 90° returns it to the initial form without rotation, and the rotation of the equilateral triangle by 120° returns it to the initial form. The rotation of the two objects provided Gaussian modulations of electric images irrespective of the rotation angle, whereas the peak position and peak amplitude changed depending on the rotation angles.

Figure 7a, c shows the effects of rotations of two square objects on the peak amplitude of electric images. These objects had each side length of 20 and 30 mm and were placed at four different lateral distances. The peak amplitude for a distance was normalized such that the maximum peak amplitude has the value of 1.0. The peak amplitudes for the two square objects exhibited the similar dependences for the rotation angles: they decreased for the rotation angles of 0° to a certain angle between 60° and 70°, and then increased for the further increase in angles. The dependence of peak amplitude is mainly due to a corner of the square which is closest to the electric organ and directed to the organ. The spatial relation between the locations of an object and the electric organ is shown in Fig. 1. The peak amplitude has the maximum value when the rotation angle is 0° because the corner A is in the closest distance from the electric organ and is directed to the organ, as shown in Fig. 7e. The peak amplitude is almost unchanged in the rotation of 0°–20° because the corner A is still close to the organ. The further rotation up to 75° allows the corner A to move far away from the organ and its direction to deviate from that to the organ, thereby occurring the attenuation of the peak amplitude. Object rotation from 75° to 85°, on the other hand, increased the peak amplitude because the corner B, adjacent to the corner A, approaches the initial position of the corner A, as shown in Fig. 7e. Furthermore, the dependence curves had the properties characteristic to lateral distance. Especially, the dependence for the distance of 10 mm exhibited a 'convex–concave' curve, and the convex profile was reduced with increasing the lateral distance. Moreover, the peak magnitude of troughs in these curves was significantly decreased for the lateral distance of 10 mm, and gradually decreased for the distances larger than 20 mm. The rotation angle at which each curve has the minimum value was slightly shifted to a lower angle with increasing the lateral distance. The first derivatives of these peak-amplitude curves are shown in Fig. 7b, d, respectively. Except for the lateral distance of 10 mm, the derivatives increased for the range of 0°–20°, and then remained almost unchanged up to the angle of 60°, and increased for further increase in angle.

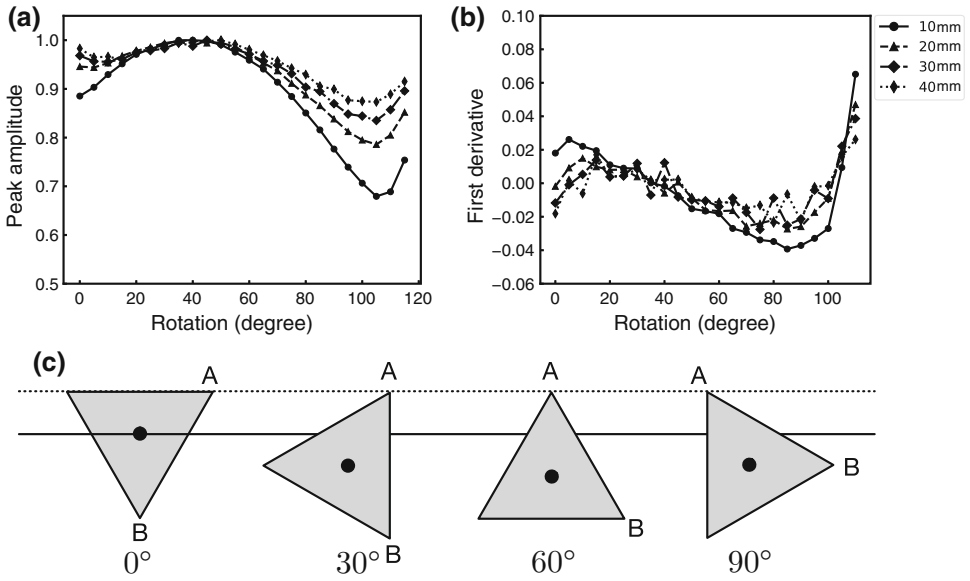

Fig. 8 Angle dependences for normalized peak amplitude of electric image and their first derivatives in rotation of an equilateral-triangle object. The triangle with each side of 30 mm was rotated around the object center located at the rostro-caudal position of 50 mm. The electric images are shown for four lateral distances of 10, 20, 30, and 40 mm. The panels, **a**–**c** are shown in the similar way to Fig. 7

For the distance of 10 mm, the peak amplitude decreased linearly up to a certain angle of around 60°, and then rapidly increased.

Figure 8a, b shows the dependence of the peak amplitude on rotation angle of an equilateral-triangle object and the first derivative of the dependence curves, respectively. The object was placed at four different lateral distances. The peak amplitudes in Fig. 8a were normalized in the similar way to Fig. 7a, c. The curves of the peak amplitudes and derivatives exhibited different dependencies from those of the squares. The peak amplitudes were gradually increased for the angles of 0°–40° and showed the steep decreases up to a certain angle nearly 100°, and then were steeply increased. The triangle object exhibited a strong convex–concave profile for the lateral distance of 10 mm. The profile was also held for the increase in the lateral distance, although the profile was weakened with the increase in distance. The derivatives showed gradual increases for the angles of 0°–10°, and then decreases up to a certain angle nearly 90°, and then the steep increases. The dependence of the peak amplitude can be explained by a corner of the triangle which is closest to the electric organ and directed to the organ. The peak amplitude increased for the rotation angles of 0° to 40° because the corner A is closer to the electric organ and more oriented to the organ, as shown in Fig. 8c. The object rotations by 40° to 105° further reduced the peak amplitude, as the corner A moves far away from the organ and its direction is largely deviated from that to the organ. The peak amplitude increased again when the corner B is approaching the initial position of the corner A, as shown in Fig. 8c. The crucial difference in the angle dependence between the derivatives elicited by the squares and the triangle is the changes for the angles of 20°–60° when the objects were placed at the lateral distances larger than 20 mm: almost unchanged patterns evoked by the squares and the decreased patterns elicited by the triangle. The convex–concave profile of the squares appeared for the closest distance and this profile disappeared for further increase in the distance, whereas the profile of the equilateral triangle was held for different distances. The difference may be caused by the difference of the object' shape; the convex–concave profile of the squares is more weakened for further increasing the distance because the corner angle of the square is not acute. On the other hand, the profile does not disappear because the acute corner angle of the triangle causes a more rapid change of the effective area that makes a dominant contribution of electric image formation. Hence the convex–concave curve may be a characteristic profile for objects with acute corner angles.

Figure 9a shows the angle dependences of HMW of electric images for the rotations of the two squares and the triangle. The widths evoked by these objects showed the similar dependences on the rotation angle. For the lateral distance of 10 mm, the HMWs evoked by these objects decreased with the increase in the rotation angle, and then unchanged, and then increased with further increasing the rotation angle. The increase in each HMW formed a peak of the curve or a bump. The bump evoked by each object appears at the specific angle that gives the minimum value of the peak amplitude. Further increase in the lateral distance showed the dependence similar to that for 10 mm but produced a weaker dependence of HMW on the rotation angle. Figure 9b shows the rostro-caudal shifts of the peak positions elicited by the three objects. The three objects gave the similar shifts in combination with the changes of the respective peak amplitudes: the peak positions moved to the caudal side with increasing the rotation angle, and then moved to the opposite side, and then to the caudal side for further increase in rotation angle. Thus,

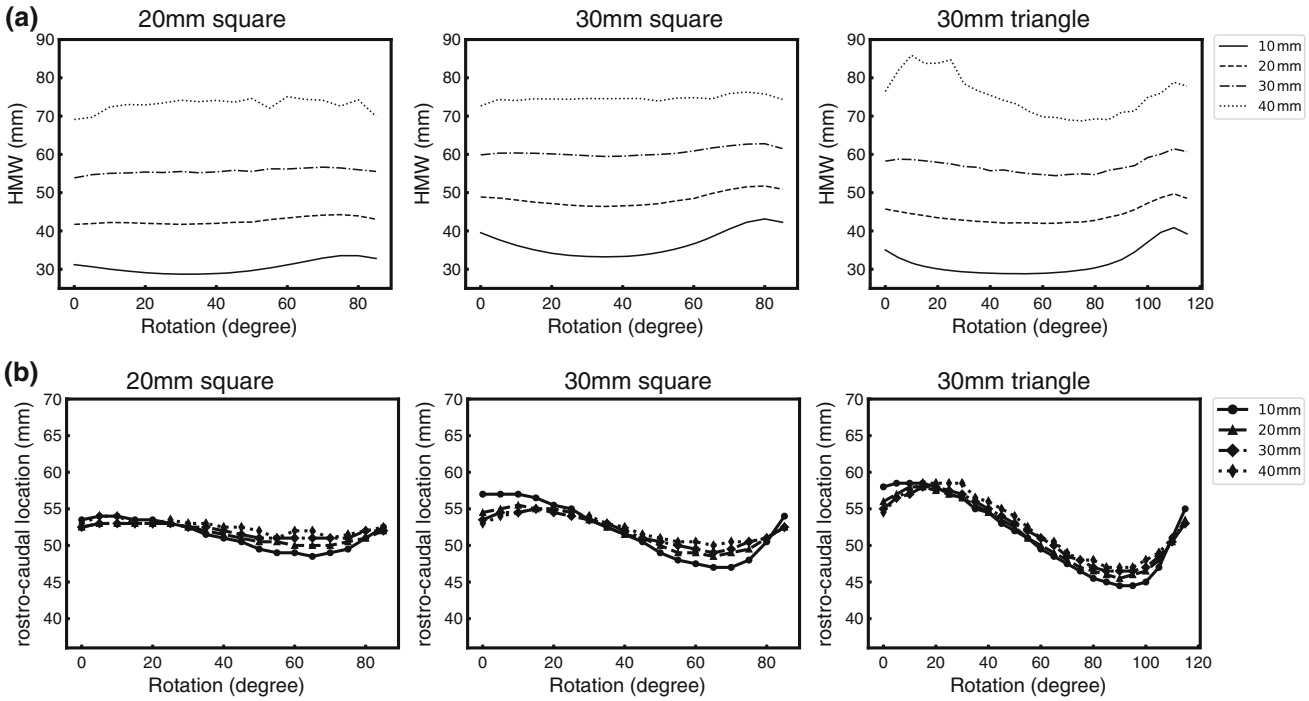

Fig. 9 Dependences of HMW and peak position of the electric image on rotations of three objects. The HMW (**a**) and peak position (**b**) were calculated under the same condition as in Figs. 7 and 8

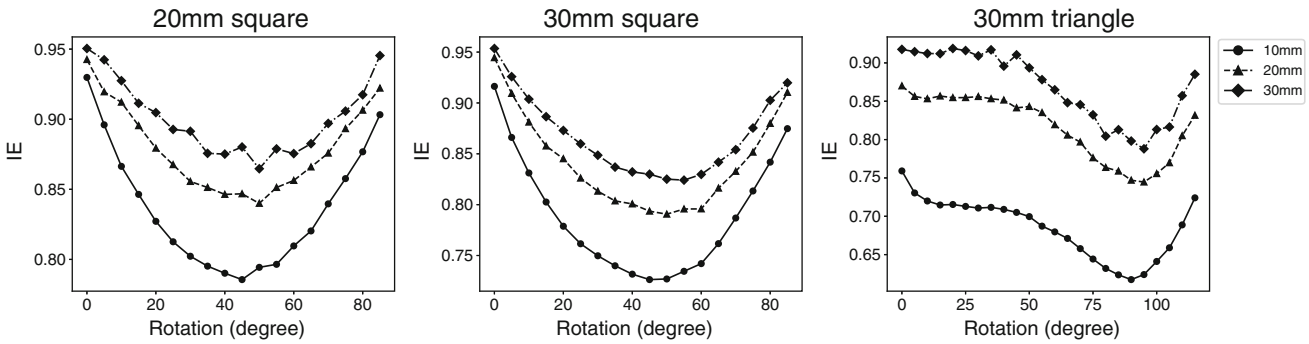

Fig. 10 Integration effects of the peak amplitude and HMW of the electric images for three objects. IE means the integration effect, given by the multiplication of normalized peak amplitude and normalized HMW. The IEs of the three objects have the angle dependences specific to the object shapes, irrespective of lateral distance

the changes of HMW and peak position provide the similar patterns irrespective of object shape but the bump of HMWs and the shift change of the peak position occur at an angle specific to the shape of each object.

Figure 10 illustrates the integration effects of peak amplitude and HMW for three objects. The effect is represented by the multiplication of the changes of the peak amplitude and HMW during an object rotation and indicates the degree of which the change of the peak amplitude is correlated with that of HMW. In the multiplication in each rotation of an object, the values of HMW shown in Fig. 9a were transformed to the values relative to the maximum value of HMW, and the normalized values were multiplied by the values of peak amplitude shown in Figs. 7 and 8. The two squares with different sizes yielded "U-type" dependences on the rotation angles irrespective of variations of the object's size and lateral distance. The integration effects for the two objects decreased with increasing the rotation angle, and then had the minimum at a certain angle nearly 45°, and then increased for further increase in the rotation angle. The integration effect for the triangle object, on the other hand, exhibited "convex–concave"—type dependences irrespective of lateral distance, as shown in Fig. 10. The rotation of triangle object maintained a large integration effect up to nearly 45° and then decreased with increasing the rotation angle and gave the minimum value at 90°, and increased with the object rotation returning to the initial form. Thus the integration effects of these objects exhibited the angle dependences character-

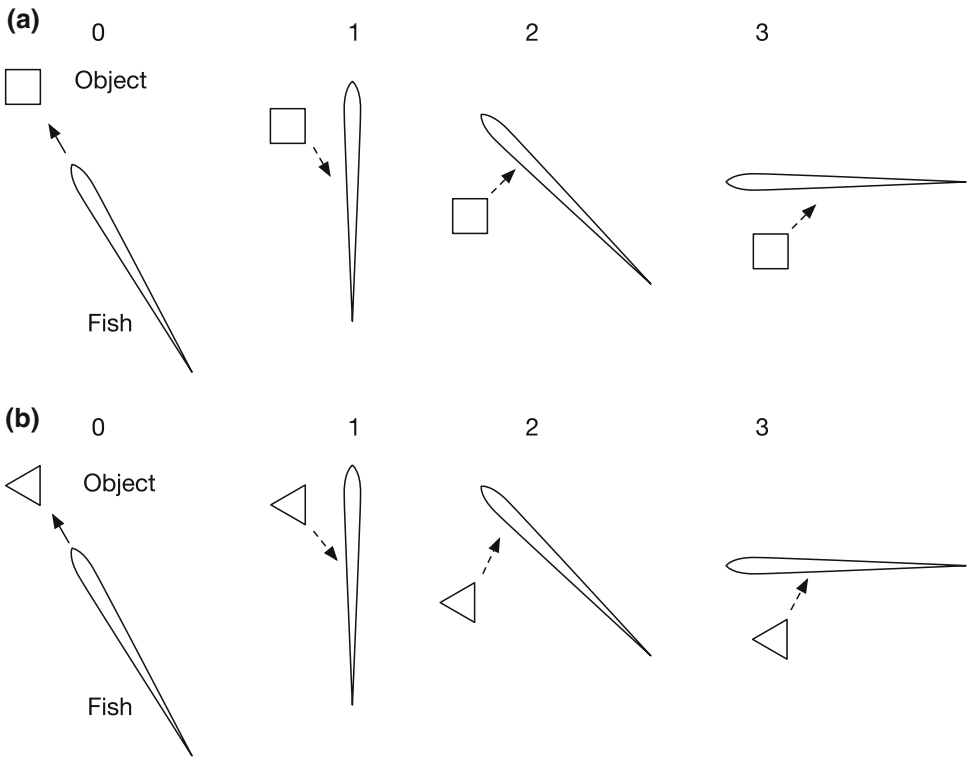

Fig. 11 Movements of weakly electric fish during exploratory behavior. A fish approaches a target object and performs a rotation movement around the object to have multiple electric images for different "electrosensory views". The behavior for a square (**a**) and an equilateral-triangle object (**b**). The dashed arrows indicate the directions of the corner that is closest to the electric organ. The electric image is enhanced when the corner is oriented to the organ ("1" and "3") and reduced when it moves far away from the organ ("2")

istic to object shapes, indicating that the effect could be an invariant measure for information of object shapes.

The results by object rotations in our model suggest that the fish may utilize their rotation movement around a target object in order to generate multiple electric images required for discrimination between object shapes. The temporal course of the image features at various angles produced by movement could be essential for the extraction of shape information. Movement of weakly electric fish is known to play important roles in the enhancement of image signal (Heiligenberg 1975; Assad et al. 1999; Chen et al. 2005), formation of electrosensory flow (Engelmann et al. 2008), and separation of a tiny target object from background scene (Babineau et al. 2006). Experimental studies have demonstrated a rotation movement of mormyrid fish in probing acts of a target object (Toerring and Belbenoit 1979; Toerring and Moller 1984). In the rotation movement, the fish maintain characteristic distances from the object, consistent with the situation of our model in which an object is rotated in such a way that the minimum distance between an object and the fish skin surface is maintained. The fish approach a target object and then change their position and orientation according to their rotation movement, as shown in Fig. 11a. The effect of the object on the electric image varies depending on the relative angles made by the orientations of the object and the electric organ. The effect increases when a corner of the object is oriented toward the electric organ ("1" and "3" in Fig. 11a), and it reduces when the corner moves far away from the organ ("2" in Fig. 11a). The exploratory behavior for an equilateral triangle is also similar to that for the square object, as shown in Fig. 11b.

3.4 Modulations of electric images for rotation of elongated objects

Figure 12a, b shows the electric images generated by the rotation of a rectangular and an ellipsoidal object, respectively. The rectangular object has the side lengths of 40 and 10 mm and the ellipsoidal object has the long axis of 40 mm and the short one of 10 mm. These objects were initially arranged in such a way that the long axis of these objects is in parallel with the longitudinal axis of the fish. This arrangement is defined as the rotation angle of 0° and both objects are returned to the initial forms by the rotation of 180°. These objects, placed at the lateral distance of 20 mm, produced slightly distorted Gaussian images for each lateral distance. The peak amplitude of electric image elicited by the rectangle object was increased with increasing the rotation angles of 0°–90° and then decreased for further rotation (95°). The ellipsoid produced the increase in the peak amplitude for the rotations of 0°–75°, and then the reduction for further rotation (90°).

Figure 13a, b shows the dependences of the peak amplitude of the electric image on the rotation angle of the rectangular and ellipsoidal objects and the first derivatives of the dependence curves, respectively. The peak amplitude was normalized in the similar way to Fig. 7. For the rectangle

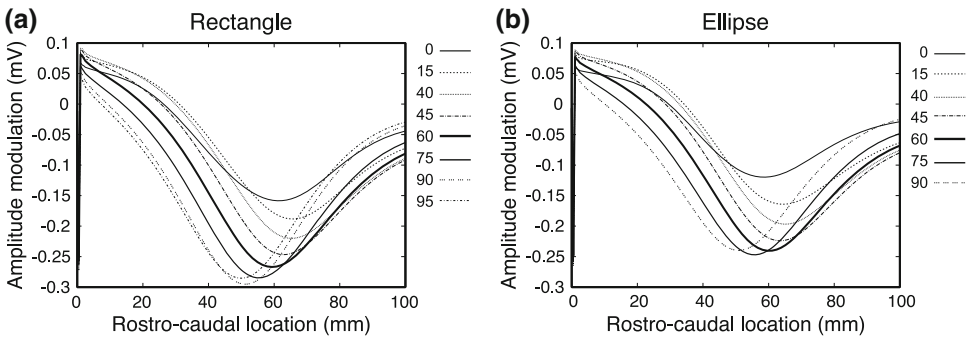

Fig. 12 Electric images generated by the rotation of two elongated objects. **a** A rectangular object with a side length of 40 and 10 mm, and **b** an ellipsoid with the long axis of 40 mm and short one of 10 mm. Rotation angles were varied in the range of 0° to 95° (**a**), and in that of 0° to 90° (**b**)

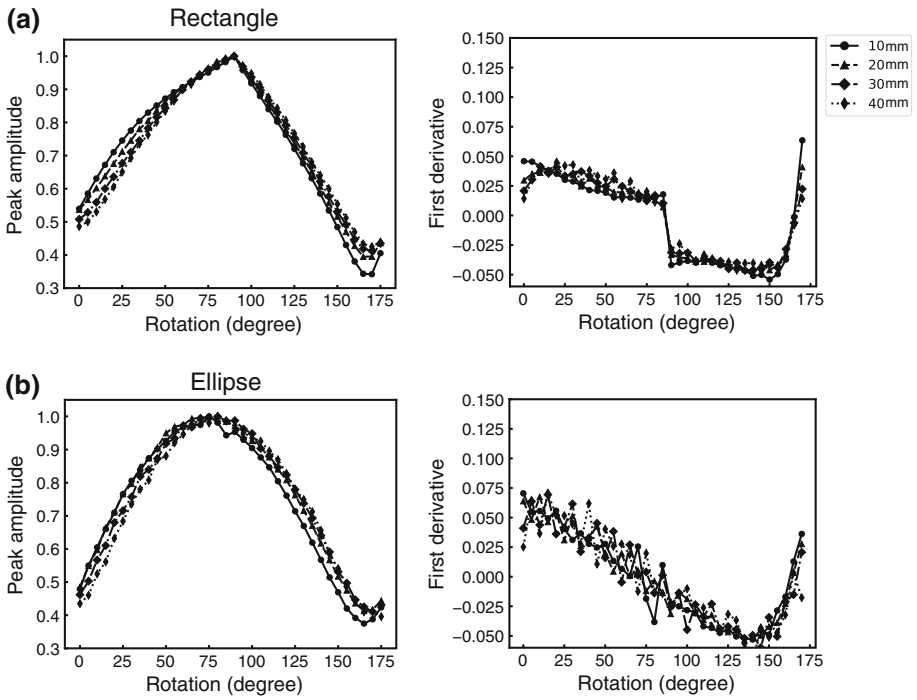

Fig. 13 Angle dependences for normalized peak amplitude of electric image and their first derivatives in rotations of two elongated objects. **a** A rectangular object. **b** An ellipsoidal object. These objects are the same as those used in Fig. 12. The dependence is shown for the lateral distances of 10, 20, 30, and 40 mm

object, the peak amplitude was increased by the rotation of 0°–90° and then decreased and further increased rapidly just before the object is returned to the initial form. The increase in the peak amplitude in the range of 0°–90° approaches a linear dependence as the lateral distance is increased. There was also a discontinuous change in the dependence curve of the peak amplitude, characterized by 'tent' shapes, as shown in Fig. 13a. A tiny deviation from 90° induces the discontinuous change between the increase and decrease in the peak amplitude. By contrast, the ellipsoid showed the dependence different from that of the rectangle object, as shown in Fig. 13b. The peak amplitude increased up to about 75°, and then decreased, and further increased just before the object returns to the initial form. The dependence showed a nonlinear shape, or 'a convex–concave' shape. The maximum and minimum angles were almost unchanged for different distances. The derivatives also showed nearly linear dependences of rotation angle for different distances. Furthermore, the dependences of the peak amplitude for the ellipsoidal object had no discontinuous point, in contrast to the dependences of the rectangle object. The presence of corners or rounded edges in the elongated objects may determine the dependence of the peak amplitude on the rotation angle.

Figure 14a shows the effects of the rotations of the rectangle and ellipsoid objects on the HMW of electric images. For the rectangle object, the dependence of HMW for the distances of 10 and 20 mm remained almost unchanged for 0°–150° and showed a bump in the range of 150°–180°. The dependence for the lateral distances of 30–40 mm provided the dependences different from those for the distances of 10 and 20 mm. The ellipsoid showed the dependences similar to the rectangle object but bump disappeared. The changes of the peak position for the rotation of these objects are shown in Fig. 14b. The rotation of the rectangle object caused the peak shifts toward the caudal side for the angles of 0°–25°, and then those toward the rostral side up to a certain angle around 150°, and those toward the caudal side for further

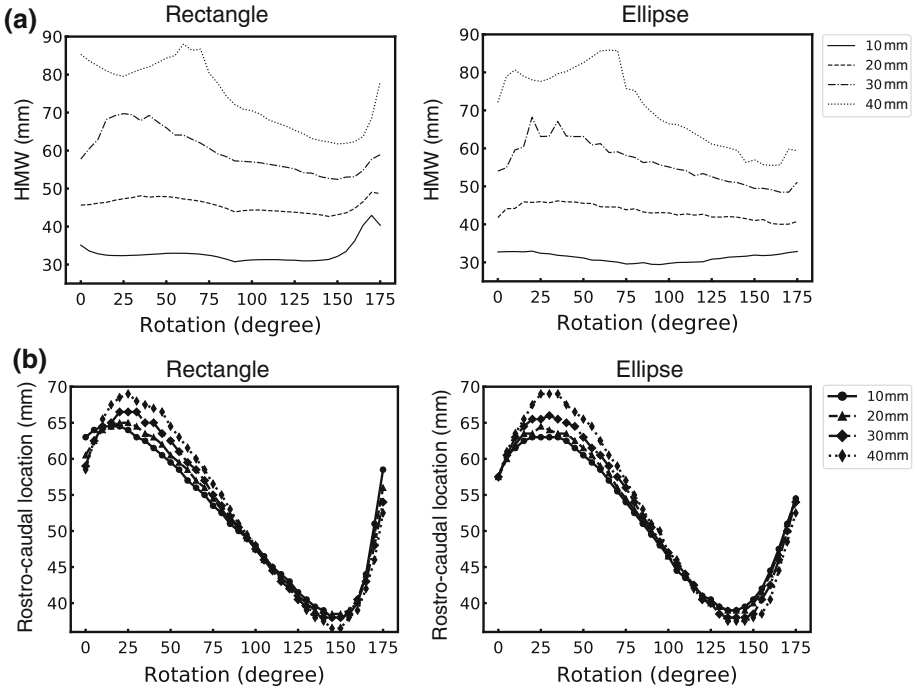

Fig. 14 Changes of HMW and peak position for rotations of a rectangle and an ellipsoidal object. **a** HMW. **b** Peak position. The changes are shown for the lateral distances of 10, 20, 30, and 40 mm. The HMW and peak position were calculated under the same condition as in Fig. 13

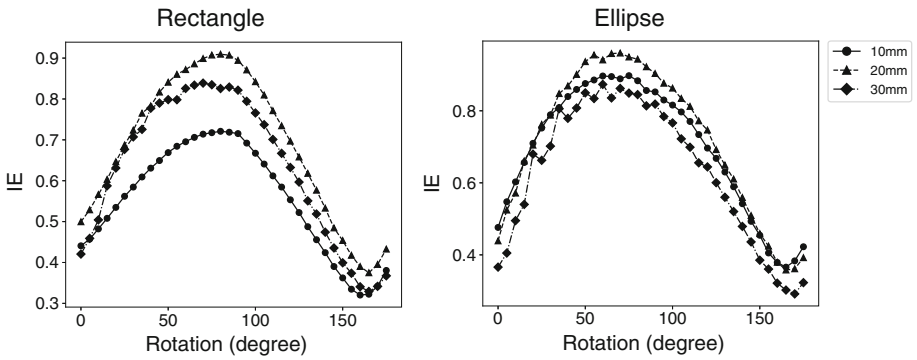

Fig. 15 Integration effects of the peak amplitude and HMW for two elongated objects. The integration effects, IEs, show the angle dependences characteristic to the two object shapes, independently of lateral distance

rotation. The ellipsoid also showed the peak shifts similar to the rectangle object.

The integration effects for the rectangular and ellipsoidal objects are shown in Fig. 15. These objects caused, as a whole, "inversed-U" type dependences on rotation angles, although a small increase appeared in the right side of each of the dependence curves. The rectangle object had the maximum integration effect at the angle of 80°, and the ellipse object allowed the maximum effect to shift toward a lower angle. The difference in the angles may come from the difference in object shapes of whether the object has corners or rounded edges. Thus the integration effects of the elongated objects provide the angle dependences specific to object shapes, supporting the idea that the effects could be an invariant measure for shape information.

4 Discussion

To study the electric-image features critical for shape discrimination of objects, we made a hypothesis that shape information of an object is not represented by a single electric image but by multiple images caused by the fish movement around the object. To test the hypothesis, we developed a computational model that can predict the electric field around a weakly electric fish and the electric images for the rotation of differently shaped objects. We found three main results. First, objects of different shapes exhibit similar Gaussian shapes in single electric images and provide little significant difference in the images. Second, the rotations of these objects produce various changes in the peak amplitude, HMW, and peak position of images, specific to geometric features of objects such as acute corners, rounded edges, and spatial anisotropy. These changes depend on the distance and size of an object. Third, despite the various changes of such features of an electric image, the integrated effect of the peak

amplitude and HMW provides an angle dependence characteristic to each object's shape, indicating that the effect could be an invariant measure for discriminating between objects of different shapes. Thus shape information may be determined through an active behavior of the fish such as rotation movement around an object. The shape discrimination based on 'blurred images' in the electrosensory system is in contrast to that based on accurate images in a visual system, but it is similar to visual recognition in the sense that object information is represented by multiple images produced by different viewpoints.

In the studies of electrolocation, it is important to elucidate what features of electric images represent object features such as distance, size, shape, and electric property. The relationship between object's distance and its size and electric image has been investigated by modeling studies (Rasnow 1996; Assad et al. 1999; Chen et al. 2005) and behavioral study (von der Emde 1998). In a wave-type fish, the relative width of electric image changes depending on the lateral distance of an object, but it remains constant for various sizes of the object (Assad et al. 1999). In a pulse-type fish, the maximum slope normalized to the maximum amplitude in electric images is shown to be an essential feature for determining object's distance (von der Emde et al. 1998). In contrast, there has been so far no detailed studies on difference in electric images of differently shaped objects. Although preliminary studies have been made, the relationship between object shape and electric image still remains unclear. Schwarz (2000) measured one-dimensional cross sections of electric images of objects of different shapes (cubes, spheres, and pyramids), but found no unambiguous cues that encode object shape. Also, the ability to discriminate between differently shaped objects has been demonstrated in a two-alternative, force-choice procedure in a pulse-type fish, *G. petersii* (von der Emde and Fetz 2007; von der Emde et al. 2010). The behavioral study suggested that the fish are able to link local features of an electrolocation pattern to represent object's shape. In the present study, we have shown that the peak amplitude, width, and peak position of electric images over the object's rotation have the angle dependences depending on objects' shapes and lateral distances, and offered that the integration effect of the peak amplitude and HMW in object rotation could be an essential quantity for discriminating between differently shaped objects. The features of electric images and the integration effect, presented here, may provide clues for analyzing the results of physiological and behavioral experiments for shape discrimination.

Movement of fish plays an important role in object perception in electrolocation because sensing is an active process. Some forms of body movement are used to shape sensory input. Tail-bending behavior enhances spatial contrast of a target signal (Heiligenberg 1975), and helps separate object shape from position (Bacher 1983). The specific movements, caused by a tail-probing behavior of the *Eigenmannia*, modulate the amplitude of an object image, allowing the fish to disambiguate the image features (Assad 1997). Moreover, back-and-forth movement nearby a target object contributes to the separation of a target signal from the signal of a large object such as rocks and the river bottom (Babineau et al. 2007). Recent studies demonstrated that a pulse-type fish, *G. Petersii*, utilizes sensorimotor integration of the electric flow (electrosensory input patterns) to detect object distance (Hofmann et al. 2013, 2017). Furthermore, the experimental study of the fish, *G. Petersii*, showed that movements of the fish in backgrounds enable object discrimination up to a farther distance (Fechler and von der Emde 2013). Clarke et al. (2014) found a role of motion reverse in contrast coding of an object in the electrosense of gymnotiform fish, *Apteronotus leptorhynchus*. Our model incorporates the rotation of objects of different shapes, and shows that the rotation movement of the fish around an object may be utilized to produce multiple electric images necessary for shape discrimination. Rotation movements are observed in probing acts of a target object in mormyrid fish (Toerring and Belbenoit 1979; Toerring and Moller 1984). Moreover, behaviors other than the rotation movement may also contribute to shape discrimination. In our model, an acute corner of equilateral triangle generates the similar angle dependences of the peak amplitude of electric image for different lateral distances, while the corner effect of a square reduces with increasing the distance. This suggests that looming and receding motions may provide a cue of whether an object has an acute corner. In addition, contrast enhancement of image features, caused by back-and-forth movement, may be also involved in shape discrimination. The coupling of several movements appears essential for discriminating object shape, in addition to distance and size.

Several models have been developed to study the electric fields involved in active electrolocation. They are based on analytical methods (Bacher 1983; Rasnow and Bower 1996; Assad et al. 1999; Chen et al. 2005), Finite-difference methods (Heiligenberg 1975; Caputi et al. 1998; Budelli and Caputi 2000), 2D-Finite Element Methods (FEM) (Heiligenberg 1975; Hoshimiya et al. 1980; Babineau et al. 2006), and the Boundary Element Methods (BEM) (Assad 1997; Assad et al. 1999; Rother et al. 2003; Migliaro et al. 2005). These methods showed the electric-image features representing object distance, size, and impedance. However, there are few modeling studies for electric images generated by different object shapes. The present model is based on our previous model (Fujita and Kashimori 2010), but the mesh space can be formed in a self-organized manner to obtain the accurate solution of electric fields for any shape of object. Besides, as mentioned in the model section, our model can obtain efficiently accurate solution by solving directly a large size

of simultaneous equations for the electric potentials of the meshes. Our model provides a systematic method for solving accurate solution of the electric field when the geometry of an object and the environment are given. However, we have several issues to be considered. First, our model is a 2D-model and not a 3D-model. 3D-FEM simulation requires a large amount of computation and thus is not practical. 2D-FEM model is easily tractable and can catch the essential property of the electric images caused by differently shaped objects. Second, we used a rectangular shape of fish. Previous studies examined electric images using the models mimicking realistic fish body (Assad et al. 1999; Rother et al. 2003; Chen et al. 2005; Migliaro et al. 2005; Babineau et al. 2006, 2007). It has been demonstrated that a tapered fish body is responsible for the formation of homogeneous electric fields in the rostral half of the body (Babineau et al. 2006). Although the shape of the fish body is one of the important factors for determining electric field around the fish body, the difference in the shape of a fish body would not change the qualitative property of the electric field. Third, our model has a uniform skin conductivity, whose value is the same as that at the head. The fish has actually the skin conductivity non-uniformly distributed over the skin, constructed with a low conductivity at the head and a high conductivity in the tail region. A model of a fish body with a uniform conductivity at the head has been shown to produce little change in electric image shape in the rostral half of the fish body compared with that produced by a model with a non-uniform skin conductivity (Babineau et al. 2006). Finally, our model assumes a simple spatio-temporal pattern of electric organ, as seen in the *Eigenmannia*. For more complex patterns of electric organ, we need to extend our model to a more complex model that incorporates the property of the patterns. It remains to be inspected how these simplifications described above affect the results of the electric images produced by objects of different shapes.

In the present study, we have shown the profile of the angle dependences of electric image features, such as the peak amplitude, HMW, and peak position, during object rotation. We have shown further that the integration effect of the peak amplitude and HMW provides the angle dependence characteristic to each object shape. The next step in our study is to investigate how the angle dependences of the electric-image features are represented in the neural circuits of the fish, and how the integration effect is decoded. These angle dependences mean the temporal dependences of these features because an object or the fish rotates with an angular velocity. The temporal changes of these features are first encoded by electroreceptors embedded in fish skin surface. Electric stimulus with the temporal changes evokes spatiotemporal activity of receptor afferents. Furthermore, afferents project topographically to electrosensory lateral-line lobe (ELL) (Heiligenberg 1991). E-type cells receive directly excitatory input from electroreceptors (Berman and Maler 1998). The same electroreceptor afferents are also sending input to I-type cells via local inhibitory interneurons. The E- and I-type cells, respectively, encode the increase and decrease in temporal inputs from electroreceptor afferents, and thus may be responsible for representing shape information. These cells have been shown to participate in a contrast coding of a spatiotemporal electric signal caused by a motion reverse of weakly electric fish (Clarke et al. 2014). In encoding of shape information, ELL neurons transform the spatiotemporal activity of afferents to more sophisticated spatiotemporal activity, i.e., spatiotemporal burst activity. The change of the peak amplitude would be encoded into the dynamic properties of burst spikes such as interburst intervals and burst timing, whereas the change of HMW would be reflected in the temporal change of the width of spatiotemporal burst activity in ELL. The integration effect of electric-image features could be decoded by the integration of these burst features in ELL activity, probably implemented by a higher area such as the torus. We presented a neural model of the electroreceptor-ELL system whose spike and burst dynamics can represent distance and size information of an object (Fujita and Kashimori 2006; Fujita et al. 2007). Combining the neural model with the results of electric images presented here, we will study the neural mechanism by which shape information is represented in the receptors-ELL system of weakly electric fish.

Acknowledgements This work was supported by JSPS KAKENHI Grant Number 15K07146.

Compliance with ethical standards

Human and animal rights This article does not contain any studies with human participants or animals performed by any of the authors.

References

Alamir M, Omar O, Servagent N, Girin A, Bellemain P, Lebastard V, Gossiaux PB, Boyer F, Bouvier S (2010) On solving inverse problems for electric fish like robots. In: Proceedings of the 2010 ieee international conference on robotics and biomimetics. IEEE, pp 1081–1086

Ammari H, Boulier T, Garnier J (2013) Modeling active electrolocation in weakly electric fish. SIAM J Imaging Sci 6:285–321

Assad C (1997) Electric field maps and boundary element simulations of electrolocation in weakly electric fish. Ph.D. thesis, California Institute of Technology, USA

Assad C, Rasnow B, Stoddard PK, Bower JM (1998) The electric organ discharges of the gymnotiform fishes: II. *Eigenmannia*. J Comp Physiol A 183:419–32

Assad C, Rasnow B, Stoddard PK (1999) Electric organ discharges and electric images during electrolocation. J Exp Biol 202:1185–1193

Babineau D, Longtin A, Lewis JE (2006) Modeling the electric field of weakly electric fish. J Exp Biol 209:3636–3651

Babineau D, Lewis JE, Longtin A (2007) Spatial acuity and prey detection in weakly electric fish. PLoS Comput Biol 3(3):e38

Bacher M (1983) A new method for the simulation of electric fields, generated by electric fish, and their distorsions by objects. Biol Cybern 47:51–58

Bai Y, Snyder JB, Peshkin M, MacIver MA (2015) Finding and identifying simple objects underwater with active electrosense. Int J Robot Res 34:1255–1277

Bai Y, Neveln ID, Peshkin M, MacIver MA (2016) Enhanced detection performance in electrosense through capacitive sensing. Bioinspiration Biomim 11(5):055001

Bastian J (1981) Electrolocation. I. How the electroreceptors of apteronotus albifrons code for moving objects and other electrical stimuli. J Comp Physiol A 144:465–479

Bazeille S, Lebastard V, Lanneau S, Boyer F (2017) Model based object localization and shape estimation using electric sense on underwater robots. IFAC-PapersOnLine 50:5047–5054

Bazeille S, Lebastard V, Boyer F (2018) Underwater robots equipped with artificial electric sense for the exploration of unconventional aquatic niches. Springer, Cham, pp 29–50

Berman NJ, Maler L (1998) Inhibition evoked from primary afferents in the electrosensory lateral line lobe of the weakly electric fish (*Apteronotus leptorhynchus*). J Neurophysiol 80:3173–3196

Boulier T (2013) Modeling active electrolocation in weakly electric fishes. Ph.D. thesis, École Polytechnique

Boyer F, Lebastard V (2018) Electric sensing for underwater navigation. In: Prescott TJ, Lepora N, Verschure PFMJ (eds) Living machines: a handbook of research in biomimetics and biohybrid systems. Oxford University Press, Oxford **(chapter 19)**

Boyer F, Gossiaux PB, Jawad B, Lebastard V, Porez M (2012) Model for a sensor inspired by electric fish. IEEE Trans Robot 28:492–505

Boyer F, Lebastard V, Chevallereau C, Servagent N (2013) Underwater reflex navigation in confined environment based on electric sense. IEEE Trans on Robotics 29(4):945–956

Budelli R, Caputi AA (2000) The electric image in weakly electric fish: perception of objects of complex impedance. J Exp Biol 203:481–492

Caputi AA, Budelli R, Grant K, Bell CC (1998) The electric image in weakly electric fish: physical images of resistive objects in gnathonemus petersii. J Exp Biol 201:2115–2128

Chen L, House JL, Krahe R, Nelson ME (2005) Modeling signal and background components of electrosensory scenes. J Comp Physiol A 191:331–345

Clarke SE, Longtin A, Maler L (2014) A neural code for looming and receding motion is distributed over a population of electrosensory ON and OFF contrast cells. J Neurosci 34:5583–5594

Engelmann J, Bacelo J, Metzen M, Pusch R, Bouton B, Migliaro A, Caputi A, Budelli R, Grant K, von der Emde G (2008) Electric imaging through active electrolocation: implication for the analysis of complex scenes. Biol Cybern 98:519–539

Fechler K, von der Emde G (2013) Figure-ground separation during active electrolocation in the weakly electric fish, Gnathonemus petersii. J Physiol Paris 107(1–2):72–83

Fujita K, Kashimori Y (2006) Population coding of electrosensory stimulus in receptor network. Neurocomput 69(10–12):1206–1210

Fujita K, Kashimori Y (2010) Modeling the electric image produced by objects with complex impedance in weakly electric fish. Biol Cybern 103:105–118

Fujita K, Kashimori Y, Kambara T (2007) Spatiotemporal burst coding for extracting features of spatiotemporally varying stimuli. Biol Cybern 97:293–305

Heiligenberg W (1975) Theoretical and experimental approaches to spatial aspects of electrolocation. J Comp physiol 103(3):247–272

Heiligenberg W (1991) Neural nets in electric fish. MIT press, Cambridge

Hofmann V, Sanguinetti-Scheck JI, Knzel S, Geurten B, Gmez-Sena L, Engelmann J (2013) Sensory flow shaped by active sensing: sensorimotor strategies in electric fish. J Exp Biol 216:2487–2500

Hofmann V, Sanguinetti-Scheck JI, Gmez-Sena L, Engelmann J (2017) Sensory flow as a basis for a novel distance cue in freely behaving electric fish. J Neurosci 37:302–312

Hoshimiya N, Shogen K, Matsuo T, Chichibu S (1980) TheApteronotus EOD field: waveform and EOD field simulation. J Comp Physiol 135:283–290

Lanneau S (2017) Model based localization and estimation of an ellipsoidal object using artificial electric sense. Ph.D. thesis, Ecole nationale supérieure Mines-Télécom Atlantique

Lanneau S, Lebastard V, Boyer F (2016) Object shape recognition using elec-tric sense and ellipsoid's polarization tensor. In: 2016 IEEE International Conference on Robotics and Automation (ICRA), Stockholm, Sweden, pp 4692–4699

Lebastard V, Chevallereau C, Girin A, Boyer F, Gossiaux PB (2012) Localization of small objects with electric sense based on kalman filter. In: 2012 IEEE international conference on robotics and automation, Saint Paul, MN, USA, pp 1137–1142

Lebastard V, Chevallereau C, Girin A, Servagent N, Gossiaux PB, Boyer F (2013) Environment reconstruction and navigation with electric sense based on a kalman filter. Int J Robot Res 32:172–188

Lebastard V, Boyer F, Lanneau S (2016) Reactive underwater object inspection based on artificial electric sense. Bioinspiration Biomim 11:45003–45003

Lewis RW, Nithiarasu P, Seetharamu KN (2004) Fundamentals of the finite element method for heat and fluid flow. Wiley, Hoboken

Lissmann HW, Machin KE (1958) The mechanism of object location in *Gymnarchus niloticus* and similar fish. J Exp Biol 35:451–486

Migliaro A, Caputi AA, Budelli R (2005) Theoretical analysis of prereceptor image conditioning in weakly electric fish. PLoS Comput Biol 1(2):123–131

Rasnow B (1996) The effects of simple objects on the electric field of apteronotus. J Comp Physiol A 178:397–411

Rasnow B, Bower B (1996) The electric organ discharges of the gymnotiform fishes: I. *Apteronotus leptorhynchus*. J Comp Physiol A 178:383–396

Rother D, Migliaro A, Canetti R, Gmez L, Caputi A, Budelli R (2003) Electric images of two low resistance objects in weakly electric fish. Bio Syst 71:169–177

Schwarz S (2000) *Gnathonemus petersii*: three-dimensional object shape detection and the geometry of the selfproduced electric field. Ph.D. thesis, Zoological Institute, University of Bonn, Germany

Solberg JR, Lynch KM, MacIver MA (2008) Active electrolocation for underwater target localization. Int J Robot Res 27:529–548

Toerring MJ, Belbenoit P (1979) Motor programmes and electroreception in mormyrid fish. Behav Ecol Sociobiol 4:369–379

Toerring MJ, Moller P (1984) Locomotor and electric displays associated with electrolocation during exploratory behavior in mormyrid fish. Behav Brain Res 12(3):291–306

von der Emde G (1998) Capacitance detection in the wave-type electric fish *Eigenmannia* during active electrolocation. J Comp Physiol A 182:217–224

von der Emde G, Fetz S (2007) Distance, shape and more: recognition of object features during active electrolocation in a weakly electric fish. J Exp Biol 210:3082–3095

von der Emde G, Schwarz S, Gomez L, Budelli R, Grant K (1998) Electric fish measure distance in the dark. Nature 395:890–894

von der Emde G, Behr K, Bouton B, Engelmann J, Fetz S, Folde C (2010) 3-Dimensional scene perception during active electrolocation in a weakly electric pulse fish. Front Behav Neurosci 4:26